# Wideband Single Carrier Transmitter Configuration Equalizing Non-flat Frequency Response

Hiroto Yamamoto, Atsushi Fukuda, Sumire Aoki, Hiroshi Hamada, Hiroshi Okazaki, and Yasunori Suzuki
6G-IOWN Promotion Department, NTT DOCOMO, INC.
3-6 Hikarino-oka, Yokosuka-shi, Kanagawa, 239-8536 Japan
hiroto.yamamoto.mb@nttdocomo.com

***Abstract*— For wideband single carrier transmission over a bandwidth of several gigahertz, the non-flat frequency response derived from transmitter components in the operating band seriously deteriorates the transmission quality. One promising approach to address this problem is equalizing the non-flat frequency response in a transmitter. This paper proposes a novel sub-THz transmitter configuration that has a feedback route for calculating the inverse frequency response and multiplying it with a transmission signal in the frequency region. To confirm the feasibility of the proposed configuration, the transmission quality in the proposed configuration is measured and evaluated. Experimental results confirm that the proposed configuration improves the error vector magnitude value by 12 dB at 8 Gbaud.**

***Keywords—Sub-THz, Single Carrier Transmission, Wideband Transmission, Equalizing***

## I. Introduction

There are a variety of studies that have been initiated on communication technologies for the 6th generation mobile communications system (6G) [1, 2]. An extremely high data rate exceeding 100 Gbps is listed as one of the requirements for 6G [3]. According to Shannon's channel capacity equation, the data rate depends on the bandwidth, *BW*, and the signal-to-noise ratio (SNR) [4]. Increasing the number of multi-input and multi-output (MIMO) branches, *N*, is another approach for high data rate communications systems [5]. Although the data rate can increase in proportion to the *BW* and *N,* it seems that an extremely large *N* is required to meet the 6G data rate requirement for *BWs* used by the mobile communications systems so far. Therefore, expanding the *BW* is an effective approach. According to [6], a *BW* of several gigahertz is required to meet the 6G data rate requirement.

In order to utilize a wide *BW*, it is necessary to use a high frequency band. Therefore, the use of the 150-GHz band and 300-GHz band, which are representative of sub-terahertz frequencies, is being considered [7]. There are some concerns regarding the design and manufacture of transmission devices for such a high frequency band, for example, discussion on superiority among transmission schemes such as single carrier transmission and multi-carrier transmission. It is considered that the required output backoff of a power amplifier for single carrier transmission is lower than that for multi-carrier transmission [8].

On the other hand, for a wideband single carrier transmission over several gigahertz, the non-flat frequency response derived from transmitter components causes inter-symbol interference and seriously deteriorates the transmission quality [9]. Frequency response flatness of the transmitter components can be designed and achieved individually in conventional narrowband operation. However, this becomes difficult to achieve over a *BW* of several gigahertz because flatness design considering the parasitic elements of each device is required for an unprecedented wide *BW* in the high frequency band. To the best of our knowledge, a wideband single carrier transmitter with a configuration that achieves frequency response flatness has not yet been proposed.

In this paper, a novel transmitter configuration that achieves frequency response flatness is proposed. The transmitter implements a functionality for equalizing the non-flat frequency response caused by transmitter components included in intermediate frequency (IF) and radio frequency (RF) devices. To confirm the feasibility of the proposed transmitter, the transmission quality is measured and evaluated. Experimental results show improvement based on eye diagrams and error vector magnitude (EVM) values for transmission signals modulated using the 64QAM scheme.

## II. Proposed Transmitter Configuration

Fig. 1 shows a block diagram of the proposed transmitter configuration. Transmitters basically comprise a baseband signal generator, frequency up-converter, filters, a power amplifier, and antenna. The baseband signal generator generates a single carrier modulation signal. In Fig. 1, $X(f)$ denotes the spectrum of the generated signal. The frequency of the transmission signal is up-converted to an RF signal. The spectrum of the RF transmission signal depends on the amplitude and phase characteristics, $H(f)$, of the transmission devices such as the frequency up-converter, filters, and amplifier in Fig. 1. For wideband single carrier transmissions, a non-flat frequency response causes inter-symbol interference and deteriorates the transmission quality. The proposed transmitter has a feedback route for the transmission signal that minimizes the inter-symbol interference caused by the non-flat frequency response. The output signal of the filter after amplification is partially coupled to the feedback route using a coupler and then frequency down-converted. The feedback transmission signal is employed to calculate the inverse frequency response, $H^{-1}(f)$. The inverse frequency response is multiplied in the frequency region with the baseband signal to equalize the non-flat frequency response after passing through the RF devices.

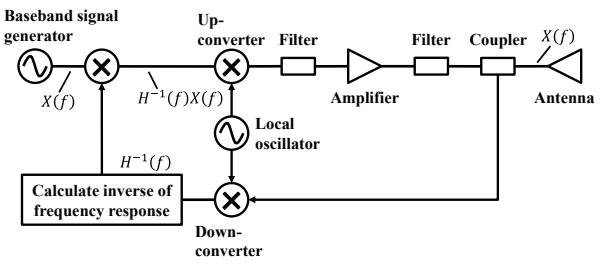


Fig. 1. Block diagram of proposed transmitter configuration.

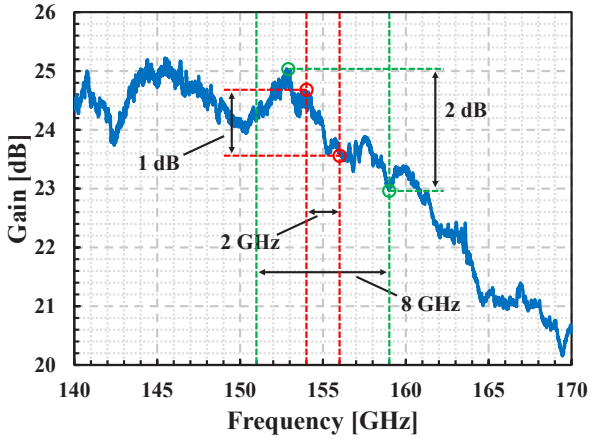


Fig. 2. Measured small signal gain of D-band amplifier.

Fig. 2 shows the measured small signal gain characteristics of a commercially available D-band amplifier. According to Fig. 2, the gain decreases gradually as the operating frequency increases. For example, when the transmission signal has a *BW* of 2 GHz at the center frequency of 155 GHz, the amplitude deviation is 1 dB. However, the amplitude deviation is 2 dB for the transmission *BW* of 8 GHz and becomes larger than that for 2 GHz.

Not only the frequency characteristics of the amplifier, but also those of the other RF devices such as the filters and frequency up-converter are taken into account to equalize the non-flat frequency response of the transmitter. Therefore, the inverse frequency response is calculated from the total frequency responses of the transmission devices. The frequency response comprises the amplitude and phase characteristics. Needless to say, not only the amplitude characteristics as shown in Fig. 2 but also the phase characteristics are required for equalization. The transmission signal from the baseband signal generator is then multiplied in the frequency region using the inverse frequency response so that the inter-symbol interference can be minimized after passing through the transmission devices.

## III. Experimental Results

To confirm the feasibility of the proposed configuration, the transmission quality in terms of eye diagrams and the EVM is measured and evaluated. Figs. 3(a) and 3(b) show experimental block diagrams for the conventional and proposed configurations, respectively. The proposed configuration has a feedback route that multiplies the inverse frequency response of the RF devices in the frequency region to the baseband signal. The wideband single carrier transmission signal with the IF of 8.5 GHz is generated using an arbitrary waveform generator (AWG) (M8195A, Keysight). Then, the frequency of the signal is converted to the RF of 155 GHz using the up-converter. A high-pass filter (HPF) rejects the image signal generated during frequency conversion and leaked signals from the local oscillator. Then, the transmission signal is amplified. The attenuation level of the attenuator is set to correspond to the coupling factor of the coupler in Fig. 1. Then, the RF transmission feedback signal is converted to an IF using the down-converter. An inverse frequency response is obtained from the total frequency response of the

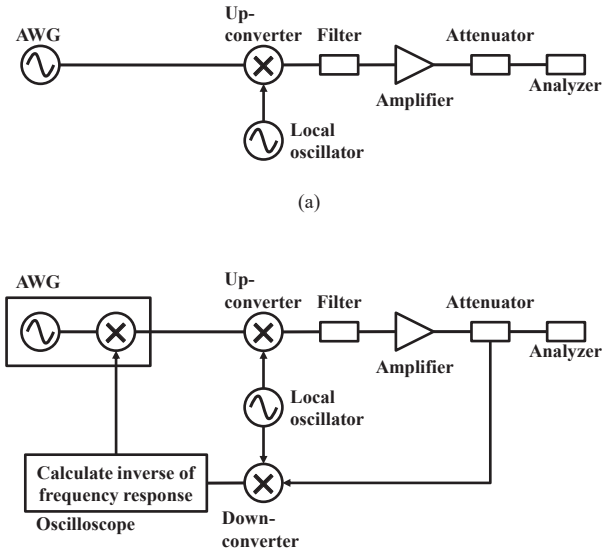


Fig. 3. Block diagrams of (a) conventional and (b) proposed experiment configurations.

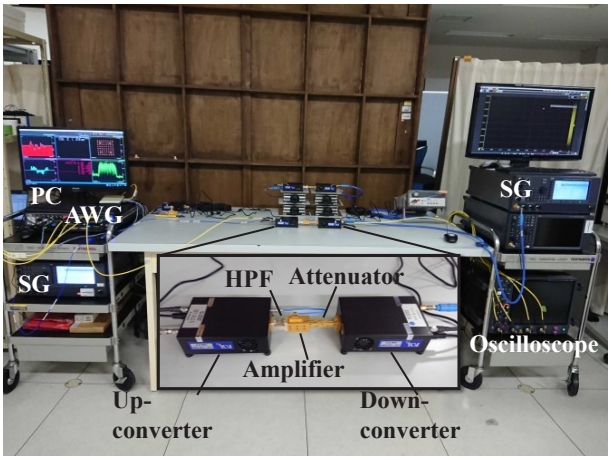


Fig. 4. Experimental configuration.

RF devices using an oscilloscope (UXR-0334A, Keysight). In this experiment, the inverse frequency response can be calculated using a zero-forcing algorithm that equalizes the feedback signal with inter-symbol interference. The inverse frequency response is multiplied in the frequency region with the transmission signal and an equalizing transmission signal is generated using the AWG. Fig. 4 shows a picture of the experimental configuration. The AWG and oscilloscope are operated using a PC. The figure shows the up-converter (WR6.5CCU-M4, VDI) and down-converter (WR6.5CCD-M4, VDI) that are employed.

Tab. 1 gives the experimental parameters. The transmission signal has the roll-off factor, $\alpha$, of 0.2. The actual signal *BW* is calculated using the equation below;

$$BW = Baud\ rate \times (1 + \alpha). \quad (1)$$

TABLE I. EXPERIMENTAL PARAMETERS

| | |
|---|---|
| Baud rate [Gbaud] | 2, 4, 6, 8 |
| Roll-off factor | 0.2 |
| Modulation scheme | 64QAM |
| Carrier frequency of IF [GHz] | 8.5 |
| Carrier frequency of RF [GHz] | 155.0 |

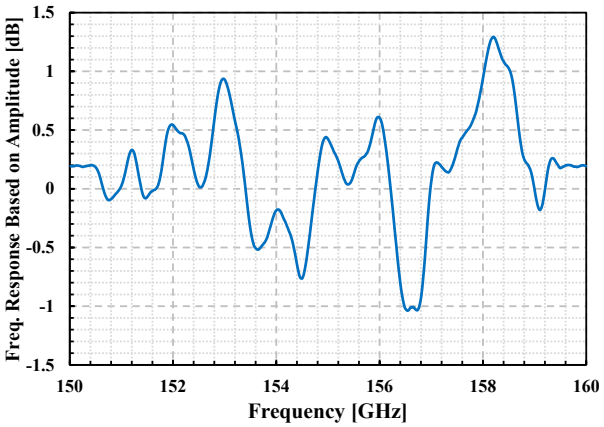


Fig. 5. Inverse frequency response based on amplitude for baud rate of 8 Gbaud.

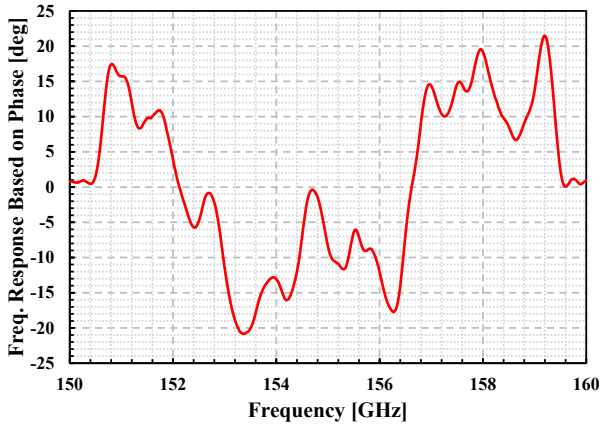


Fig. 6. Inverse frequency response based on phase for baud rate of 8 Gbaud.

According to (1), *BW*s with the baud rates of 2, 4, 6, and 8 Gbaud are 2.4, 4.8, 7.2 and 9.6 GHz, respectively. The transmission signal is modulated using the 64QAM scheme. The IF and RF of the system are 8.5 GHz and 155 GHz, respectively.

Fig. 5 shows the calculated inverse frequency response based on the amplitude for the baud rate of 8 Gbaud. According to Fig. 5, amplitude deviation within ±1.3 dB is observed in the actual *BW* from 150.2 GHz to 159.8 GHz corresponding to 8 Gbaud.

Fig. 6 shows the calculated inverse frequency response based on phase for the baud rate of 8 Gbaud. According to the figure, phase deviation within ±22 degrees is observed in the same *BW*.

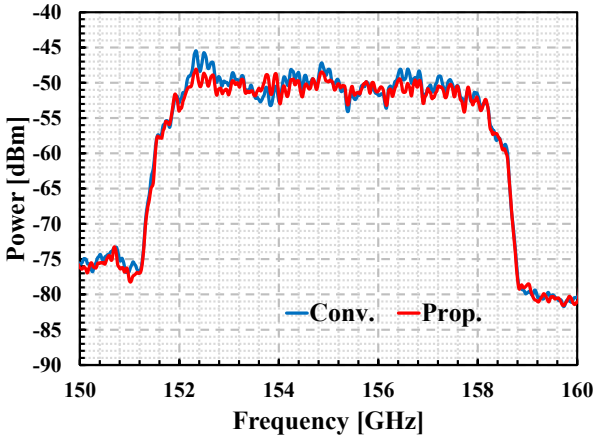


Fig. 7. Spectra of transmission signal for conventional and proposed configurations for baud rate of 8 Gbaud.

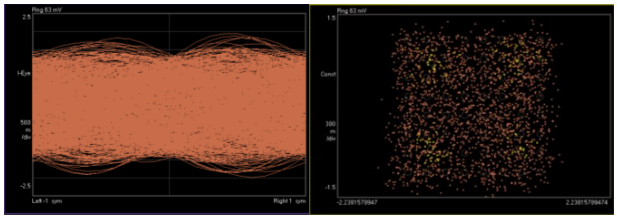

(a)

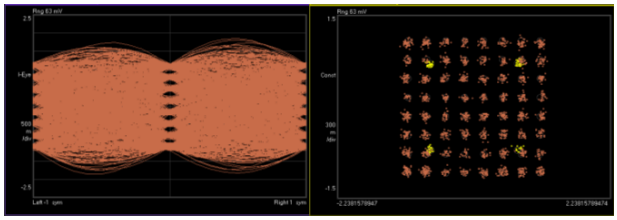

(b)

Fig. 8. Eye diagrams and constellations for (a) conventional and (b) proposed configurations.

Fig. 7 shows the spectra of the transmission signal for the conventional and proposed configurations in Figs. 3(a) and 3(b), respectively, for the baud rate of 8 Gbaud. According to Fig. 7, the frequency response deviations of the proposed configuration are approximately 2.5 dB lower than that for the conventional configuration.

Figs. 8(a) and 8(b) show eye diagrams and constellations for the conventional and proposed configurations, respectively, for the baud rate of 8 Gbaud. The eye diagrams for the conventional configuration are closed resulting from waveform distortion due to inter-symbol interference as shown in Fig. 8(a). On the other hand, the eye diagrams for the proposed configuration are opened as shown in Fig. 8(b) because the inter-symbol interference is minimized. Additionally, according to the constellation diagrams, we confirm that the proposed configuration achieves the 64QAM

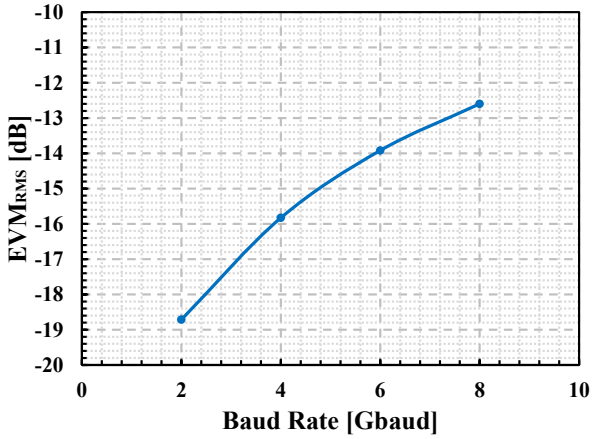


Fig. 9. $EVM_{RMS}$ of conventional configuration.

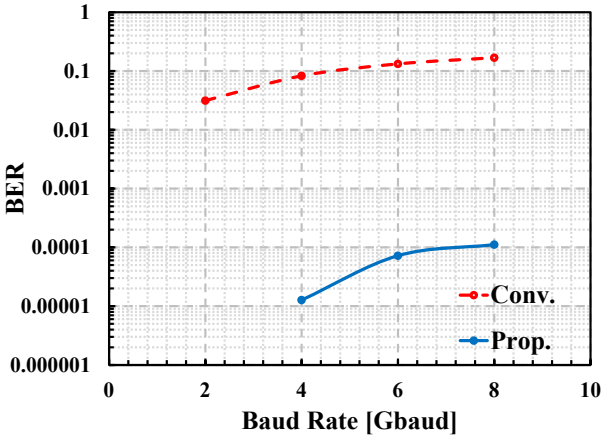


Fig. 11. BER of proposed configuration.

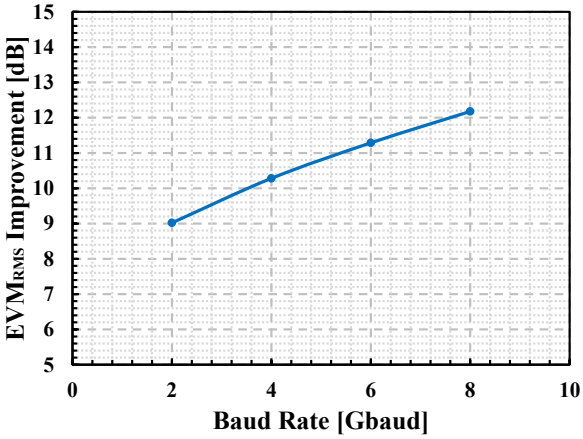


Fig. 10. Improvement in $EVM_{RMS}$ using proposed configuration.

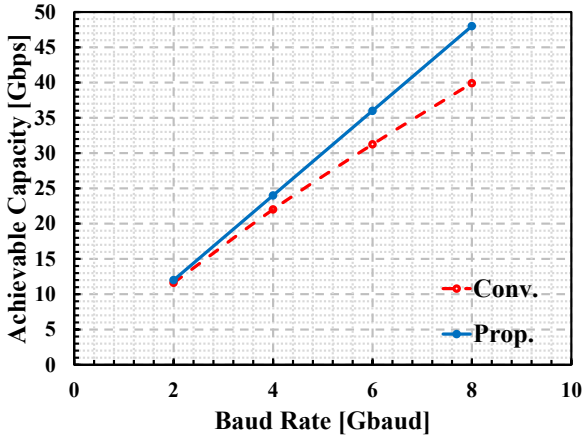


Fig. 12. Achievable capacity improvement of proposed configuration.

constellation using the feedback route to multiply the inverse frequency response.

Fig. 9 shows the measured $EVM_{RMS}$ values for the conventional configuration shown in Fig. 3(a) corresponding to the baud rate and modulation scheme. The $EVM_{RMS}$ is defined as

$$EVM_{RMS} = \frac{\sqrt{\frac{1}{N}\sum_{i}^{N}\left|S_{ideal,i} - S_{meas,i}\right|^2}}{\sqrt{\frac{1}{M}\sum_{i=1}^{M}\left|S_{ideal,i}\right|^2}}. \qquad (2)$$

where $i$ and $N$ denote the symbol index and the number of symbols, respectively. Term $M$ denotes the number of the constellation points. Terms $S_{ideal}$ and $S_{meas}$ denote the location of the ideal signal points and measured signal point, respectively. According to Fig. 9, the higher the baud rate that is set, the worse the $EVM_{RMS}$ becomes. This is why higher baud rates result in lower power densities in the case of constant transmission power regardless of the baud rate. In addition, because the deviations in amplitude and phase become large for high baud rates as explained in relation to Fig. 2, the SNR is decreased due to inter-symbol interference.

Fig. 10 shows the amount of $EVM_{RMS}$ improvement using the proposed configuration with the feedback route to multiply the inverse frequency response. According to Fig. 10, the amount of improvement is large for a high baud rate. For example, the improvement of 9 dB from the $EVM_{RMS}$ of -18.7 dB is obtained for the baud rate of 2 Gbaud. On the other hand, the improvement of 12 dB from the $EVM_{RMS}$ of -12.6 dB is obtained for the baud rate of 8 Gbaud. As the deviations in amplitude and phase become large for a high baud rate as shown in Fig. 2, equalizing the non-flat frequency response for a wideband signal is more valuable than that for a narrowband signal for a single carrier transmitter.

Fig. 11 shows the measured bit error rates (BERs). In this measurement, no error correction code is used. In Fig. 11, the dashed line and the solid line represent the BER of the conventional and proposed configurations, respectively. Here, the BER of the proposed configuration for the baud rate of 2 Gbaud is error free. According to Fig. 11, the BER of the proposed configuration is less than 0.0001.

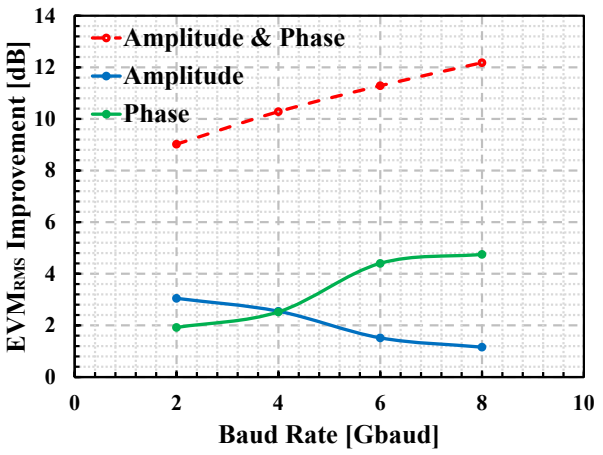


Fig. 13. Amount of $EVM_{RMS}$ improvement by multiplying inverse frequency response that considers amplitude and phase characteristics.

Fig. 12 shows the achievable capacity improvement for the proposed configuration. The capacity is calculated by using the following equation;

$$Capasity = Baud\ rate\ \times (1 - BER). \qquad (3)$$

In Fig. 12, the dashed line and solid line represent the bit rates of the conventional and proposed configurations, respectively. Based on Fig. 12, we confirm that the proposed configuration achieves the capacity improvement of 8 Gbps at 8 Gbaud employing the 64QAM scheme.

Fig. 13 shows the effect of considering both amplitude and phase characteristics to calculate the inverse frequency response. In Fig. 13, the red dashed line represents the $EVM_{RMS}$ improvement considering the amplitude and phase characteristics. The blue and green solid lines represent the improvement considering only the amplitude characteristics and only the phase characteristics, respectively. Based on Fig. 13, both the amplitude and phase characteristics should be taken into account to obtain sufficient improvement.

## IV. Conclusion

This paper proposed a wideband single carrier transmitter configuration that implements a functionality for minimizing the inter-symbol interference caused by the non-flat frequency response resulting from the transmission devices. From the eye diagram experimental results, the proposed configuration with a feedback route that multiplies the inverse frequency response to the transmission signal in the frequency region minimizes the inter-symbol interference. The $EVM_{RMS}$ is also improved by 12 dB for the baud rate of 8 Gbaud and the 64QAM scheme. We confirmed that the proposed configuration is needed to achieve a high bit rate using a wideband single carrier transmission. Investigating the frequency characteristics of the down-converter in the feedback route is a future issue.

## Acknowledgement

This paper includes a part of results of "R&D for Expansion of Radio Wave Resources (JPJ000254)," commissioned by The Ministry of Internal Affairs and Communications, Japan.

## References

[1] W. Saad, M. Bennis, and M. Chen, "A vision of 6G wireless systems: Applications, trends, technologies, and open research problems," IEEE Network, Volume: 34, Issue: 3, pp. 134-142, October 2019.

[2] M. Giordani, M. Polese, M. Mezzavilla, S. Rangan, and M. Zorzi, "Toward 6G networks: Use cases and technologies," IEEE Communications Magazine, Volume: 58, Issue: 3, pp. 55-61, March 2020.

[3] NTT DOCOMO, INC., "White paper 5G evolution and 6G," Version 4.0, January 2022.

[4] J. Ma, "Modified Shannon's capacity for wireless communication," IEEE Microwave Magazine, Volume: 22, Issue: 9, pp. 97-100, August 2021.

[5] P. K. Agyapong, M. Iwamura, D. Staehle, W. Kiess, and A. Benjebbour, "Design considerations for a 5G network architecture," IEEE Communications Magazine, Volume: 52, Issue: 11, pp. 65-75, November 2014.

[6] P. Yang, Y. Xiao, M. Xiao, and S. Li, "6G wireless communications: Vision and potential techniques," IEEE Network, Volume: 33, Issue: 4, pp. 70-75, July 2019.

[7] T. S. Rappaport, *et al.*, "Wireless communications and applications above 100 GHz: Opportunities and challenges for 6G and beyond," IEEE Access, Volume: 7, pp. 78729-78757, June 2019.

[8] S. H. Han and J. H. Lee, "An overview of peak-to-average power ratio reduction techniques for multicarrier transmission," IEEE Wireless Communications, Volume: 12, Issue: 2, pp. 56-65, April 2005.

[9] J. L. Zamorano, J. Nsenga, W. Van Thillo, A. Bourdoux, and F. Horlin, "Impact of phase noise on OFDM and SC-CP," IEEE Global Telecommunications Conference, pp. 3822-3825, November 2007.